

Strain-modulated antiferromagnetic Chern insulator in $NiOsCl_6$ monolayer

Bin Wu(武斌), Na Li(李娜), Xin-Lian Chen(陈新莲), Wei-Xiao Ji(纪维霄), Pei-Ji Wang(王培吉), Shu-Feng Zhang(张树峰), and Chang-Wen Zhang(张昌文)
Citation: Chin. Phys. B, 2024, 33 (**12**): 127301. DOI: 10.1088/1674-1056/ad84cb
Journal homepage: http://cpb.iphy.ac.cn; http://iopscience.iop.org/cpb

What follows is a list of articles you may be interested in

Field induced Chern insulating states in twisted monolayer-bilayer graphene

Zhengwen Wang(王政文), Yingzhuo Han(韩英卓), Kenji Watanabe, Takashi Taniguchi, Yuhang Jiang(姜宇航), and Jinhai Mao(毛金海)
Chin. Phys. B, 2024, 33 (**6**): 067301. DOI: 10.1088/1674-1056/ad3b8a

Electrically controllable spin filtering in zigzag phosphorene nanoribbon based normal—antiferromagnet—normal junctions

Ruigang Li(李锐岗), Jun-Feng Liu(刘军丰), and Jun Wang(汪军)
Chin. Phys. B, 2024, 33 (**1**): 017304. DOI: 10.1088/1674-1056/acf82a

Thermal Hall effect and the Wiedemann-Franz law in Chern insulator

Anxin Wang(王安新) and Tao Qin(秦涛)
Chin. Phys. B, 2023, 32 (**10**): 107301. DOI: 10.1088/1674-1056/ace158

Two-dimensional topological semimetals

Xiaolong Feng(冯晓龙), Jiaojiao Zhu(朱娇娇), Weikang Wu(吴维康), and Shengyuan A. Yang(杨声远)
Chin. Phys. B, 2021, 30 (**10**): 107304. DOI: 10.1088/1674-1056/ac1f0c

Disorder induced phase transition in magnetic higher-order topological insulator: A machine learning study

Zixian Su(苏子贤), Yanzhuo Kang(康艳卓), Bofeng Zhang(张博峰), Zhiqiang Zhang(张智强), Hua Jiang(江华)
Chin. Phys. B, 2019, 28 (**11**): 117301. DOI: 10.1088/1674-1056/ab4582

Strain-modulated antiferromagnetic Chern insulator in $NiOsCl_6$ monolayer

Bin Wu(武斌)[†], Na Li(李娜)[†], Xin-Lian Chen(陈新莲), Wei-Xiao Ji(纪维霄), Pei-Ji Wang(王培吉), Shu-Feng Zhang(张树峰)[‡], and Chang-Wen Zhang(张昌文)[§]

School of Physics and Technology, University of Jinan, Jinan 250022, *China*

(Received 26 July 2024; revised manuscript received 1 October 2024; accepted manuscript online 9 October 2024)

Recently, Chern insulators in an antiferromagnetic (AFM) phase have been suggested theoretically and predicted in a few materials. However, the experimental observation of two-dimensional (2D) AFM quantum anomalous Hall effect is still a challenge to date. In this work, we propose that an AFM Chern insulator can be realized in a 2D monolayer of $NiOsCl_6$ modulated by a compressive strain. Strain modulation is accessible experimentally and used widely in predicting and tuning topological nontrivial phases. With first-principles calculations, we have investigated the structural, magnetic, and electronic properties of $NiOsCl_6$. Its stability has been confirmed through molecular dynamical simulations, elasticity constant, and phonon spectrum. It has a collinear AFM order, with opposite magnetic moments of 1.3 μ_B on each Ni/Os atom, respectively, and the Néel temperature is estimated to be 93 K. In the absence of strain, it functions as an AFM insulator with a direct gap with spin–orbital coupling included. Compressive strain will induce a transition from a normal insulator to a Chern insulator characterized by a Chern number $C = 1$, with a band gap of about 30 meV. This transition is accompanied by a structural distortion. Remarkably, the Chern insulator phase persists within the 3%–10% compressive strain range, offering an alternative platform for the utilization of AFM materials in spintronic devices.

Keywords: Chern insulator, antiferromagnetism, topological materials

PACS: 73.43.–f, 75.50.Ee, 71.15.Mb **DOI:** 10.1088/1674-1056/ad84cb

1. Introduction

Chern insulators, also named quantum anomalous Hall effect, is one of the magnetic topological materials, which has been a most attractive field in recent years. It allows to manipulate magnetic properties to control topological states. It begins at the discovery of quantum Hall effect and then predicted by Haldane in a toy model in the absence of external magnetic field.[1] Now, it has been extended to include both magnetic topological insulators (TIs) and semimetals. In experiments, several magnetic topological materials have been confirmed,[2] including antiferromagnetic (AFM) topological insulators, magnetic higher-order TIs, axion insulators, Chern insulators, magnetic Weyl and Dirac semimetals. Chern insulators have chiral edge states which are dissipationless and may be used in spintronic devices. Chern insulators have been mostly studied theoretically and confirmed experimentally in ferromagnetic (FM) materials.[3–20] However, it is realized that Chern insulator is possible as well in AFM material if the combined spatial and time-reversal symmetry is broken. For the time being, the AFM Chern insulator has not been observed experimentally. One reason is that the suggested candidate materials are still scarce. Therefore, it is essential to predict more potential materials to promote the development in the field of AFM Chern insulators.[21–24]

Antiferromagnetic Chern insulators have been predicted only in a few materials including: $NiXCl_6$ (X = Ru, Os),[25,26] CrO,[27] MoO,[28] $RbCr_4S_8$,[29] and Mn_3Sn.[29] Both $RbCr_4S_8$[29] and Mn_3Sn[29] are in-plane AFM metals with the global band gap lying a little away from the Fermi surface. Further doping is needed to realize the insulator phase. $NiOsCl_6$ is tuned into the Chern insulator phase by modulating the value of Hubbard U.[26] However, we notice that the allowable range of U spans only from 0 eV to 0.23 eV, posing a challenge for experimental realization. On the other hand, we notice that the nonzero Chern number in CrO,[27] MoO,[28] and $NiRuCl_6$[25] can only be induced by applying strain. Strain modulation is accessible experimentally comparing with tuning Hubbard U and it is used widely in predicting of topological phases.[30] Therefore, it is promising to modulate $NiOsCl_6$ by strain to get Chern insulator phase in a wider regime. It will help broaden the field of two-dimensional (2D) materials which have exotic properties.[31–34]

In this paper, we present a modulation scheme to achieve the AFM Chern insulator in a monolayer of $NiOsCl_6$. By maintaining a constant value of U and applying compressive biaxial strain modulation, we make a phase transition from a normal insulator to a Chern insulator. The existence of AFM Chern insulator is checked by calculating magnetic properties, analysis of band-inversion, Berry phase, Hall conductance, and topological edge states. Besides, we underline that this topological phase transition is accompanied by a structural distortion which keeps the lattice but changes the relative position

[†]These authors contributed equally to this work.
[‡]Corresponding author. E-mail: sps_zhangsf@ujn.edu.cn
[§]Corresponding author. E-mail: ss_zhangchw@ujn.edu.cn

© 2024 Chinese Physical Society and IOP Publishing Ltd

of atoms in the unit cell. As a result, there exists a sudden jump for the band gap as a function of strain at the critical point. It is different from the conventional case with only topological phase transition but no structural transition where the gap will close and reopen gradually.

2. Methods

First-principles calculations have been performed using the Vienna *ab initio* simulation package (VASP), which is based on density functional theory (DFT).[35–37] The Perdew–Burke–Ernzerhof (PBE) functional at the level of generalized gradient approximation (GGA) is used to deal with the exchange correlation interactions.[38] The correlation effects for Ni-4d and Os-5d electrons were handled by the DFT+U method with $U = 0.5$ eV for both Ni and Os atoms.[39–41] The plane-wave basis is used with a cutoff energy of 500 eV. The Brillouin zone is sampled using a Γ-centered k mesh with a size of $15 \times 15 \times 1$. The crystal structure is optimized until the force applied to each atom is less than 0.01 eV/Å. The energy convergence criterion is set to 10^{-6} eV. A vacuum layer of 20 Å is used to avoid residual interactions between adjacent layers. Berry curvature of the occupied bands is calculated by the maximally localized Wannier function method implemented in the WANNIER90 package.[42,43] Chern number is calculated with the maximal localized Wannier function tight-binding model[44] and the topological edge states are calculated using an iterative Green's function method.[45]

3. Structure and magnetism

The top and side views of the monolayer $NiOsCl_6$ lattice are shown in Fig. 1(a), with gray, brown, and green balls representing Ni, Os, and Cl atoms, respectively. In fact, this structure is similar with that of the CrI_3 monolayer, with two Cr atoms replaced by an Ni atom and an Os atom, while I atoms replaced by Cl atoms. It is a hexagonal lattice and the first Brillouin zone is shown in Fig. 1(b). It corresponds to the space group $P312$ and point group D_3^1. The relaxed lattice constants are $a = b = 6.13$ Å$= a_0$. To verify the thermodynamic stability of monolayer $NiOsCl_6$, we have calculated its molecular dynamics in a 3×3 supercell at a temperature of 300 K. The result is shown in Fig. 1(d). The time step is 1 femtosecond, the thermostat used is Nose–Hoover thermostat and the ensemble used is NVT, i.e., canonical ensemble. It is found that the total energy fluctuates only slightly during the entire simulation, but the structure never develops any instability leading to reconstruction, as confirmed by a snapshot of the atomic structure at 10^4 fs [inset of Fig. 1(d)]. The structure is found to be thermally stable at 300 K during the simulated period of time. Next, we calculate the elastic constants of the structure. We have $C_{11} = C_{22} = 29.2$ N/m, $C_{12} = 9.3$ N/m, $C_{66} = 9.9$ N/m, satisfying $C_{11}, C_{22} > 0$, $C_{11}C_{22} > C_{12}^2$, which is the criterion of mechanical stability. Besides, we have also calculated the phonon spectrum with a $4 \times 4 \times 1$ supercell, as shown in Fig. A1 of Appendix A. There is no imaginary frequency, which indicates that this structure is kinetically stable. To demonstrate the bonding properties, we have calculated the electron localization function, which is shown in Fig. 1(c). It is clear that electrons lie mainly on Cl atoms. Therefore, $NiOsCl_6$ is a typical ionic crystal.

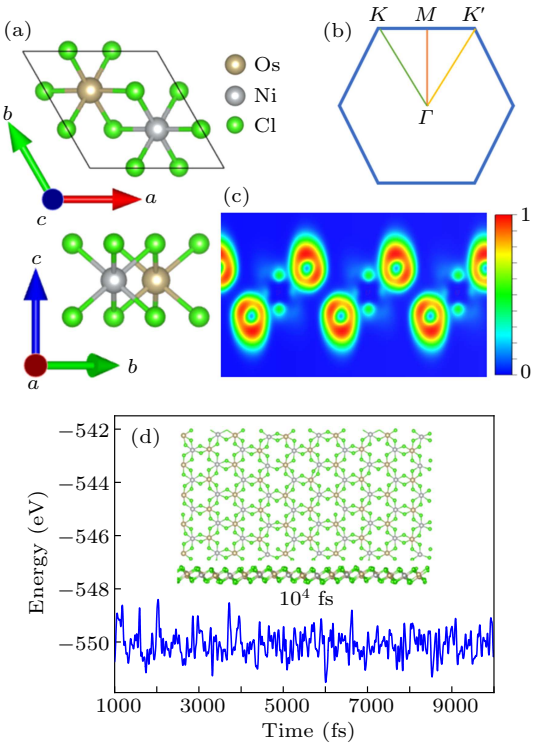


Fig. 1. (a) Top (top) and side (bottom) views of $NiOsCl_6$ monolayer, with gray balls for Os atoms, brown for Os atoms, and green for Cl atoms. (b) The first Brillouin zone and (c) electron localization function. The plane only intersects with the positions of the cores of Cl atoms. (d) Molecular dynamical evolution. The inset in panel (d) is the relaxed structure after 10^4 fs.

To determine the magnetic ground state, we have calculated the energies of several different spin configurations in a $2 \times 2 \times 1$ supercells. As shown in Fig. 2(a), the first one is an FM configuration while the other three are AFM configurations. Numerical calculations show that the AFM1 configuration has the lowest energy for the chosen magnetic configurations and therefore it suggests that AFM1 is the magnetic ground state. Further more, we have calculated the energy of the AFM1 configuration by setting spins aligned in different directions. It is found that the energy attains its minimum for spins aligned along x direction and directions rotated $\pi/3$ and $2\pi/3$ from x direction, due to the C_3^z symmetry. We calculated the magnetic anisotropic energy (MAE $= E_x - E_z$) of the AFM1 configuration, in which $E_{x/z}$ represents the energy for spins aligned at the x/z direction. The variation of MAE with biaxial strain is shown in Fig. 2(c). Since we have always $E_z > E_x$, the easy axis always lies along x direction not only for the case with no strain but also in a wide range of compressive strain $a/a_0 \in (0.9, 1)$. In order to determine the magnetic moment on each atom, we have performed Bader charge analysis

in the case with no SOC and strain. It suggests that the magnetic moment is $\pm 1.3\ \mu_B$ on Ni and Os atoms, respectively.

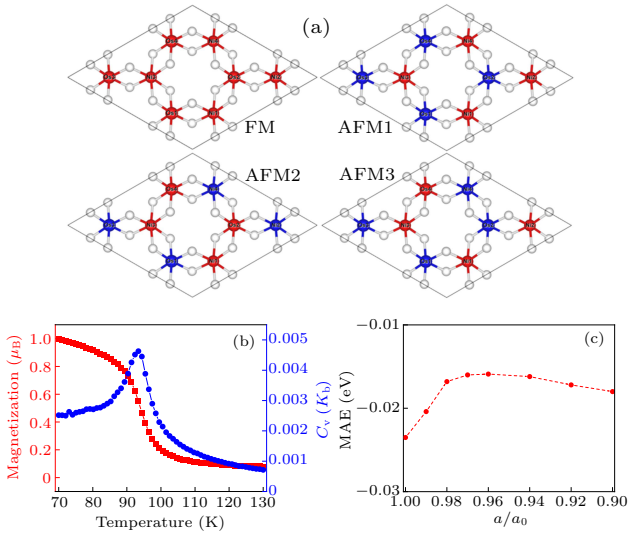


Fig. 2. (a) Four spin configurations of $NiOsCl_6$ lattice, with red, blue, and white colors representing spin up, spin down, and nonmagnetic atoms, respectively. (b) The magnetic moment (red) and specific heat capacity (blue) as the function of temperature. (c) The evolution of MAE with compressive strain.

To determine the Néel temperature of the AFM-paramagnetic phase transition, we have simulated the spin system with the Heisenberg model. The Hamiltonian is given by

$$H = -\sum_{\langle ij \rangle} \left(J^x \hat{S}_i^x \hat{S}_j^x + J^y \hat{S}_i^y \hat{S}_j^y + J^z \hat{S}_i^z \hat{S}_j^z \right), \tag{1}$$

where $S_i^{x/y/z}$ is the $x/y/z$ component of a spin vector on the i-th magnetic atom. $J^{x/y/z}$ describes the exchange coupling coefficients. The summation is over only the nearest neighboring Ni and Os sites. To determine the parameters in the model, we have calculated the energy of two spin configurations, the FM and AFM1 ones, by setting spin align at x, y, and z directions, respectively. These energies can also be expressed with parameters in the model Hamiltonian directly as

$$E_{\mathrm{FM}}^{\alpha} = E_0 - 3J^{\alpha}, \tag{2a}$$

$$E_{\mathrm{AFM1}}^{\alpha} = E_0 + 3J^{\alpha}, \tag{2b}$$

in which $\alpha = x, y, z$. Therefore, we have obtained $J^x = -5.45$ meV, $J^y = -5.43$ meV, and $J^z = -8.15$ meV. With parameters determined, we can simulate the Heisenberg spin model with Monte Carlo method. Numerical results are shown in Fig. 2(b). The red curve is the magnetic moment on an Ni/Os atom, and the blue one is the specific heat capacity. With temperature increasing, there is a sudden decrease in magnetic moment and a sharp peak in the capacity curve at about 93 K. It corresponds to the AFM–paramagnetic phase transition, and this temperature is the Néel temperature. Here we have only considered the exchange interactions between the nearest neighbors. This is reasonable since the bond length between next nearest neighbors is 6.4 Å, which is twice of that between nearest neighbors, which is 3.7 Å. It should also be noticed that Néel temperature obtained here could only be taken as an estimation since the value of exchange coefficients therefore the critical temperature predicted depends on the used functional and the value of U.[46]

On the other hand, we have aligned the magnetization along the out-of-plane direction, which is perpendicular to the easy axis lying in-plane along the x direction. Detailed numerical analysis indicates that Chern insulator phase is not allowable with the in-plane magnetization. We further consider the case of out-of-plane magnetization. In experiments, the spin polarization can be tuned to out-of-plane by magnetic field, since the MAE is only 20 meV.

4. Electronic properties

The energy band structures of $NiOsCl_6$ are shown in Fig. 3 for biaxial compressive strains $a = a_0$ and $a = 0.97a_0$, respectively. It is an AFM insulator with an indirect gap in the absence of strain and SOC, as shown in Fig. 3(a). However, energy bands of different spins are split in energy, which is different from the common AFM material. This splitting originates from that the 3d orbital of Ni atoms and 5d orbitals of Os atoms have different orbital energies.[47] Further orbital analysis indicates that the spin-up bands near Fermi level are contributed mainly by 5d orbitals of Os atoms. At finite temperature, there will be spin-up electrons and holes excited. Therefore, $NiOsCl_6$ will behave like a half metal at finite temperature. With biaxial strain $a/a_0 = 0.97$ applied, we find that the electronic band, shown in Fig. 3(c), shows similar features as that with no strain shown in Fig. 3(a).

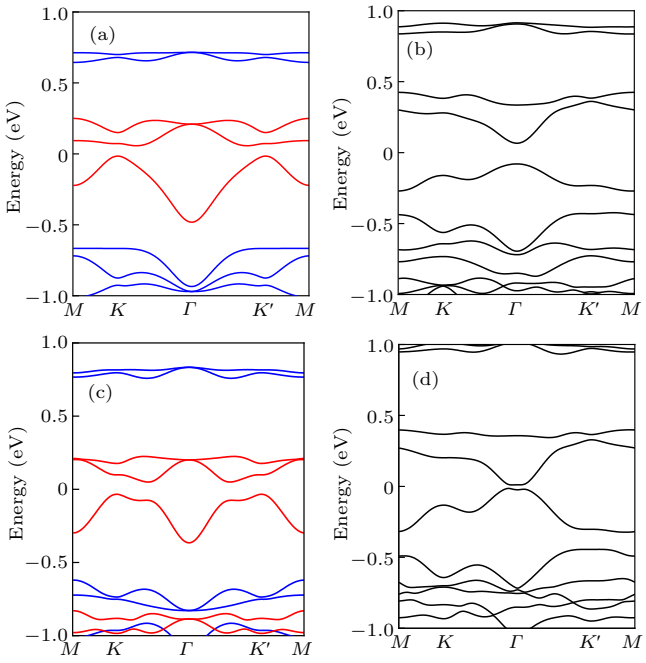


Fig. 3. Band structures of $NiOsCl_6$ without SOC (a), with SOC (b), and with strain $a/a_0 = 0.97$ without SOC (c), with SOC (d).

When SOC is taken into account, the band gap gets larger and it becomes a direct gap at Γ point as shown in Fig. 3(b) for the case with no strain. With compressive biaxial strain applied, the direct gap decreases gradually in the range $a_0 > a > a_c$ with $a_c = 0.9728$, as shown in Fig. 4.

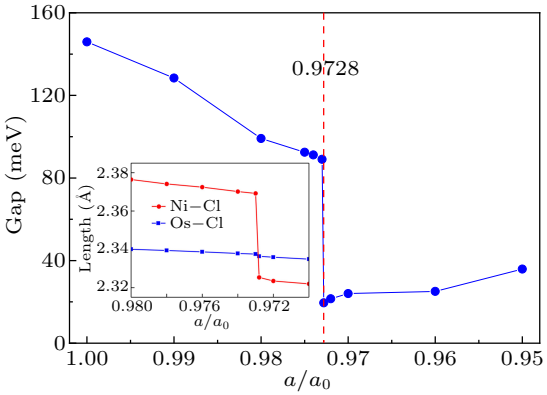


Fig. 4. Band gap variation of monolayer $NiOsCl_6$ with compressive strain in the presence of SOC. Inset is the length of Ni–Cl and Os–Cl bonds.

Interestingly, there occurs a sudden jump at $a = a_c$, which suggests a phase transition here. We notice that the space group keeps to be $P312$ in the strain range of 0%–5%. It indicates that the crystal lattice and the structure symmetry is unchanged with the phase transition. Therefore, we further study the relative position of atoms in a unit cell. Since the lengths of all six Ni/Os–Cl bonds are nearly identical, we have displayed only one Ni/Os–Cl bond in the inset of Fig. 4. It is clear that there is also a sharp change in Ni–Cl bond at $a = a_c$ while Os–Cl bond changes continuously. Remind that an Ni atom lies in a octahedral cage of Cl atoms. The sharp decrease of bond length means that Cl atoms move toward the central Ni atom and the octahedron becomes smaller. Then it is evident that a the relative position of atoms changes suddenly at $a = a_c$ while the lattice keeps unchanged. And it is this structural distortion that contributes to the gap jump.

We have plotted the energy band for $a = 0.97a_0 < a_c$ in Fig. 3(d) with SOC included. It has an indirect gap and the band looks like inverted.[48–50] It suggests that the structural distortion may be accompanied by a topological phase transition. To check this point, we have analyzed the orbital composition, Berry curvature, edge states and Hall conductance. The results are shown in Fig. 5.

Before structural distortion, $a/a_0 = 0.98$, there is no energy band inversion. It reveals that energy bands near the Fermi surface are primarily contributed by the d_{xy}, d_{z^2}, and $d_{x^2-y^2}$ orbitals as shown in Fig. 5(a). After lattice distortion, $a/a_0 = 0.97$, it is clear that there is an exchange of $d_{x^2-y^2}$ and d_{xy} orbitals at Γ point as shown in Fig. 5(a).

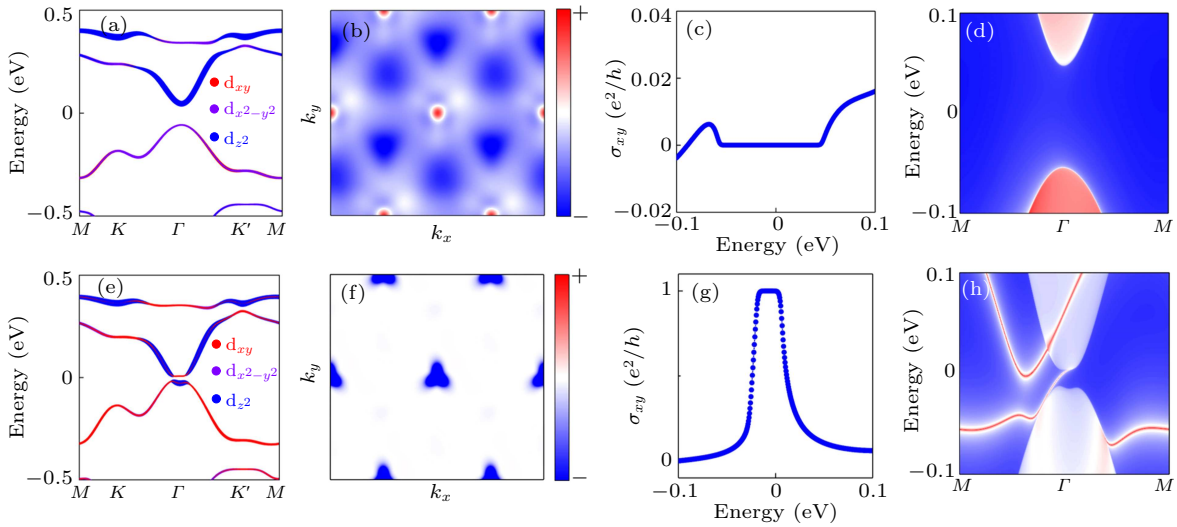


Fig. 5. Comparison of energy band orbital analysis of monolayer $NiOsCl_6$ under compressive strain (a) $a/a_0 = 0.98$, (e) $a/a_0 = 0.97$. Monolayer $NiOsCl_6$ in compression at strain $a/a_0 = 0.97$. Berry phase in the occupied state (b) $a/a_0 = 0.98$ and (f) $a/a_0 = 0.97$. Anomalous Hall conductivity versus chemical potential (c) $a/a_0 = 0.98$ and (g) $a/a_0 = 0.97$. The energy spectrum of a half-infinite structure (d) $a/a_0 = 0.98$ and (h) $a/a_0 = 0.97$.

We have also calculated Berry curvature $\Omega_z(\boldsymbol{k})$ of the occupied states, which can be expressed as

$$\Omega_z(\boldsymbol{k}) = -2\,\mathrm{Im}\sum_{m\neq n}\frac{\langle n\boldsymbol{k}|v_x|m\boldsymbol{k}\rangle\langle m\boldsymbol{k}|v_y|n\boldsymbol{k}\rangle}{(\omega_m-\omega_n)^2}, \tag{3}$$

where $\omega_{m/n}$ is the energy of the m/n-th band, $v_{x/y}$ denotes the velocity operator along x/y direction. The results are shown in Figs. 5(b) and 5(f). Before distortion, positive and negative Berry curvatures are located at Γ and K (K'), respectively. After distortion, there is only negative Berry curvature concentrated around the Γ point. And then we have calculated Hall conductance σ_{xy},[51,52] which is given by

$$\sigma_{xy} = -\frac{e^2}{h}\frac{1}{2\pi}\int_{\mathrm{BZ}}\Omega_z(\boldsymbol{k})\,\mathrm{d}^2\boldsymbol{k}, \tag{4}$$

which is just the integration of Berry curvature over the first Brillouin zone. Before distortion, shown in Fig. 5(c), Hall conductance is small and it vanishes in the bulk band gap. This

is because there is no transport channel in the gap, as shown in Fig. 5(d). After distortion, shown in Fig. 5(g), Hall conductance becomes quantized in the gap region. This conductance quantum is due to the topological edge state which connects valence and conduction bands, as shown in Fig. 5(h).

With these analysis, it is demonstrated that 2D $NiOsCl_6$ lattice film is a normal insulator in the strain regime $a_0 > a > a_c = 0.9728a_0$. It becomes a Chern insulator with $C = 1$ at least in the regime $a_c > a > 0.9a_0$. It should be underlined that this topological transition is accompanied by a structural distortion. As a result, the band gap tends to jump suddenly rather than close and reopen.

5. Conclusions

In conclusion, we have studied the structural, magnetic, and electronic properties of the 2D $NiOsCl_6$ film by first-principles calculations with the DFT+U method. The stability of this structure has been confirmed by molecular dynamics simulations, elastic constant, and phonon spectrum. Each Ni/Os atom has a magnetic moment about 1.3 μ_B, aligned collinearly to establish an AFM phase. In the absence of SOC and strain, it behaves as an insulator with an indirect gap. And only spin-up bands of 5d orbitals of Os atoms lie at Fermi surface, which makes it behave like a half-metal at finite temperature. SOC can transform it into a direct-gap insulator. Furthermore, biaxial compressive strain makes a topological phase transition from a normal insulator to a Chern insulator with a Chern number $C = 1$. This transition is accompanied by a structural distortion. As opposed to U-value modulation, strain modulation can be experimentally realized. Therefore, 2D $NiOsCl_6$ can be tuned to be an AFM Chern insulator which may provide a platform for AFM spintronics.

Appendix A: Phonon spectrum

We have also calculated the phonon spectrum with a $4 \times 4 \times 1$ supercell by the linear response approach, with parameters: IBRION=8. The result is displayed in Fig. A1. It is observed that there is no imaginary frequency, which indicates that this structure is kinetically stable.

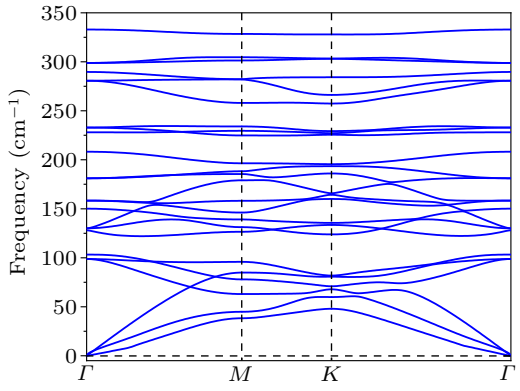


Fig. A1. Phonon spectrum of $NiOsCl_6$ monolayer.

Acknowledgments

Project supported by the National Natural Science Foundation of China (Grant Nos. 12104183, 52173283, and 62071200), the Natural Science Foundation of Shandong Province, China (Grant Nos. ZR2021MA040 and ZR2023MA091), the Taishan Scholar Program of Shandong Province, China (Grant No. ts20190939), and the Independent Cultivation Program of Innovation Team of Jinan City (Grant No. 2021GXRC043). This work was supported by high-performance computing platform at University of Jinan.

References

[1] Haldane F D M 1988 *Phy. Rev. Lett.* **61** 2015
[2] Bernevig B A, Felser C and Beidenkopf H 2022 *Nature* **603** 41
[3] Liu C X, Zhang S C and Qi X L 2016 *Annu. Rev. Conden. Matter Phys.* **7** 301
[4] Chang C Z, Liu C X and MacDonald A H 2022 *Rev. Mod. Phys.* **95** 011002
[5] Qi X L, Wu Y S and Zhang S C 2006 *Phy. Rev. B* **74** 045125
[6] Lei C and MacDonald A H 2021 *Phys. Rev. Mater.* **5** L051201
[7] Zhang J, Chang C Z, Tang P, Zhang Z, Feng X, Li K, Wang L, Chen X, Liu C, Duan W, He K, Xue Q K, Ma X and Wang Y 2013 *Science* **339** 1582
[8] Chang C Z, Tang P, Wang Y L, Feng X, Li K, Zhang Z, Wang Y, Wang L L, Chen X, Liu C, Duan W, He K, Ma X C and Xue Q K 2014 *Phys. Rev. Lett.* **112** 056801
[9] Zhang S F, Jiang H, Xie X C and Sun Q F 2014 *Phys. Rev. B* **89** 155419
[10] Polshyn H, Zhu J, Kumar M A, Zhang Y, Yang F, Tschirhart C L, Serlin M, Watanabe K, Taniguchi T, MacDonald A H and Young A F 2020 *Nature* **588** 66
[11] Sun H, Li S S, Ji W X and Zhang C W 2022 *Phys. Rev. B* **105** 195112
[12] Xiao D, Zhu W, Ran Y, Nagaosa N and Okamoto S 2011 *Nat. Commun.* **2** 596
[13] Wang J, Lian B, Zhang H, Xu Y and Zhang S C 2013 *Phys. Rev. Lett.* **111** 136801
[14] Wang Y P, Ji W X, Zhang C W, Li P, Zhang S F, Wang P J, Li S S and Yan S S 2017 *Appl. Phys. Lett.* **110** 213101
[15] Zhang S J, Zhang C W, Zhang S F, Ji W X, Li P, Wang P J, Li S S and Yan S S 2017 *Phys. Rev. B* **96** 205433
[16] Xu G, Weng H, Wang Z, Dai X and Fang Z 2011 *Phys. Rev. Lett.* **107** 186806
[17] Han Y T, Ji W X, Wang P J, Li P and Zhang C W 2023 *Nanoscale* **15** 6830
[18] Kou X, Guo S T, Fan Y, Pan L, Lang M, Jiang Y, Shao Q, Nie T, Murata K, Tang J, Wang Y, He L, Lee T K, Lee W L and Wang K L 2014 *Phys. Rev. Lett.* **113** 137201
[19] Li S S, Ji W X, Hu S J, Zhang C W and Yan S S 2017 *ACS Appl. Mater. Inter.* **9** 41443
[20] Zhang M H, Zhang C W, Wang P J and Li S S 2018 *Nanoscale* **10** 20226
[21] Hu X 2012 *Adv. Mater.* **24** 294
[22] Jungwirth T, Marti X, Wadley P and Wunderlich J 2016 *Nat. Nanotechnol.* **11** 231
[23] Baltz V, Manchon A, Tsoi M, Moriyama T, Ono T and Tserkovnyak Y 2018 *Rev. Mod. Phys.* **90** 015005
[24] Qin P, Yan H, Wang X, *et al.* 2023 *Nature* **613** 485
[25] Zhou P, Sun C Q and Sun L Z 2016 *Nano Lett.* **16** 6325
[26] Yang W W, Li L, Zhao J S, Liu X X, Deng J B, Tao X and Hu X R 2018 *J. Phys.: Condens. Matter* **30** 185501
[27] Guo P J, Liu Z X and Lu Z Y 2023 *npj Comput. Mater.* **9** 70
[28] Wu B, Song Y L, Ji W X, Wang P J, Zhang S F and Zhang C W 2023 *Phys. Rev. B* **107** 214419
[29] Liu Y T, Li J Y and Liu Q H 2023 *Nano Lett.* **23** 8650
[30] Dai Z H, Liu L Q and Zhang Z 2019 *Adv. Mater.* **31** 1805417
[31] Bafekry A, Faraji M, Fadlallah M M, Hoat D M, Jappor H R, Abdolhosseini I, Ghergherehchi M and Feghhia S A H 2021 *Phys. Chem. Chem. Phys.* **23** 25866

[32] Almayyali A O M and Jappor H R 2024 *Solid State Sciences* **150** 107483
[33] Bafekry A, Fadlallah M M, Faraji M, Hieu N N, Jappor H R, Stampfl C, Ang Y S and Ghergherehchi M 2022 *ACS Appl. Mater. Interfaces* **14** 21577
[34] Olsen T 2021 *J. Phys. D: Appl. Phys.* **54** 314001
[35] Kresse G and Hafner J 1994 *Phys. Rev. B* **49** 14251
[36] Blochl P E 1994 *Phys. Rev. B* **50** 17953
[37] Kresse G and Furthmuller J 1996 *Phys. Rev. B* **54** 11169
[38] Perdew J P, Burke K and Ernzerhof M 1996 *Phys. Rev. Lett.* **77** 3865
[39] Dudarev S L, Botton G A, Savrasov S Y, Humphreys C J and Sutton A P 1998 *Phys. Rev. B* **57** 1505
[40] Anisimov V I, Zaanen J and Andersen O K 1991 *Phys. Rev. B* **44** 943
[41] Wan X, Vishwanath A and Savrasov S Y 2012 *Phys. Rev. Lett.* **108** 146601
[42] Wang X, Yates J R, Souza I and Vanderbilt D 2006 *Phys. Rev. B* **74** 195118
[43] Mostofi A A, Yates J R, Lee Y S, Souza I, Vanderbilt D and Marzari N 2008 *Comput. Phys. Commun.* **178** 685
[44] Brouder C, Panati G, Calandra M, Mourougane C and Marzari N 2007 *Phys. Rev. Lett.* **98** 046402
[45] Sancho M P L, Sancho J M L and Rubio J 1985 *J. Phys. F: Met. Phys.* **15** 851
[46] Olsen T 2019 *MRS Commun.* **9** 1142
[47] Guo S D and Ang Y S 2023 *Phys. Rev. B* **108** L180403
[48] Xiao J W and Yan B H 2021 *Nat. Rev. Phys.* **3** 283
[49] Chege S, Ning P, Sifuna J and Amolo G O 2020 *AIP Adv.* **10** 095018
[50] Zhao M W, Zhang X M and Li L Y 2015 *Sci. Rep.* **5** 16108
[51] Jungwirth T, Niu Q and MacDonald A H 2002 *Phys. Rev. Lett.* **88** 207208
[52] Yao Y, Kleinman L, MacDonald A H, Sinova J, Jungwirth T, Wang D S, Wang E and Niu Q 2004 *Phys. Rev. Lett.* **92** 037204